THIRTEENTH EUROPEAN ROTORCRAFT FORUM

12.1
Paper No. 62

FLOW VISUALIZATION ON A HELICOPTER ROTOR IN HOVER USING ACENAPHTHENE

C.-H. ROHARDT

INSTITUTE FOR DESIGN AERODYNAMICS
DFVLR, BRAUNSCHWEIG

September 8-11, 1987

ARLES, FRANCE

ASSOCIATION AERONAUTIQUE ET ASTRONAUTIQUE DE FRANCE

FLOW VISUALIZATION ON A HELICOPTER ROTOR IN HOVER USING ACENAPHTHENE

C.-H. ROHARDT
INSTITUTE FOR DESIGN AERODYNAMICS
DFVLR, BRAUNSCHWEIG

Abstract

Results of flow visualization of the boundary layer character on a helicopter rotor blade under real conditions in hover flight are presented. Laminar boundary layers of considerable extent were detected. Comparisons of the experimental results with the transition location calculated by a two-dimensional method are discussed.

Notation

α, Alp	angle of incidence
c_a	lift coefficient
$c_{a\ max}$	maximum lift coefficient
c_m	pitching moment coefficient, related to quarter chord
c_{m0}	pitching moment coefficient at $c_a=0$
c_p	static pressure coefficient
$c_{p\ min}$	minimum static pressure coefficient
c_{p^*}	critical static pressure coefficient (Ma=1)
c_w	drag coefficient
c_{wD}	friction induced pressure drag coefficient
c_{wR}	friction drag coefficient
c_{wW}	wave drag coefficient
c_{w0}	drag coefficient at $c_a=0$
d	airfoil thickness
l	chord length
Ma	Mach number
Re	Reynolds number
x	coordinate in chordwise direction
r	local radius of rotor
R	radius of main rotor
V	local free stream velocity

1. Introduction

The philosophy in designing modern airfoils tries to find shapes with pressure distributions, which are favourable to achieve long laminar boundary layers in a wide range of angles of attack, Mach and Reynolds numbers. The laminar boundary layer reduces the friction drag and substantial gains in overall performance are possible.

In order to apply this technology to helicopter rotors it is necessary to check if laminar boundary layers occur on a real rotor under operational flight conditions.

Therefore, flow visualization experiments on a helicopter rotor in hover flight have been carried out. These tests were made on a normal blade of a MBB BO-105 helicopter of DFVLR using the sublimation technique with acenaphthene. In the following this technique is described, the application on a helicopter rotor is discussed and the results are presented together with calculations.

2. Principle of flow visualization using acenaphthene

The acenaphthene method uses a saturated solution of acenaphthene in acetone. The test surface is sprayed with this liquid, and when the solvent has vaporized, the test surface is covered by a thin, white layer of crystalline acenaphthene. Acenaphthene has the property of sublimating at normal state conditions (temperature, pressure) where the sublimation speed depends on temperature and heat flux. This effect is used to detect the transition location. In a boundary layer the wall shear stress and the heat flux depend on the character of the boundary layer. The wall shear stress and also the heat flux in a laminar boundary layer are small, whereas in the turbulent case the wall shear stress and the heat flux are large. This behaviour results in the fact, that the layer of acenaphthene crystals sublimates faster in the region of turbulent boundary layers than in a laminar one. One can then detect the beginning of the fully turbulent boundary layer at the location where the white layer of the crystals is completely removed. Thus, the laminar-turbulent transition location can easily be determined from the high contrast picture on the surface.

3. Conditions of the experiment

Tests were carried out on a rotor blade of a MBB BO-105 helicopter. It is made out of composites and carries an erosion cap at the leading edge of 18% of blade chord. The airfoil shape is a modified NACA 23012. The rotor was in use about 450 hours at time of the tests. Thus, the erosion cap was significantly roughened. Also, the transition from the cap to the rear part of the blade was not smooth due to manufacturing deficiencies.

For the tests the surface was prepared in that way, that exhaust gas residues and insect debris were removed. Afterwards the surface was sprayed with the solution of acenaphthene. It was necessary to smooth the layer of acenaphthene after spraying, because during spraying, accumulations of acenaphthene crystals developed at the nozzle and were blown to the blade surface. These small crumbs represented an additional surface roughness and had to be removed. After a two minutes warm-up at reduced rotational speed and zero lift the helicopter went over to a ten minutes hover flight followed by an additional cool-down phase equal to the warm-up. The hover flight is the only flight condition of a helicopter with a nearly constant blade lift over the rotation angle, and therefore with nearly constant pressure distributions on the blades. The flight conditions are listed in Table 1.

Photographs were taken from upper and lower surface of the rotor blade after the hover flight. Marks ④ to ⑩ were applied to the rotor blade at relative rotor radius positions between r/R=0.62 and r/R=0.98.

4. Results of the flow visualization

Fig. 1 shows the complete view of the rotor blade upper surface in radial direction from section ⑥ (r/R≈0.75) to the rotor tip. The principle details of an acenaphthene picture shall be explained using this figure. They can be seen more or less clear in each of the following photographs of the rotor blade surface.

In the front part of the blade a bright region can be seen, which is in sharp contrast to the dark, grey colour of the blade surface. The white, crystal acenaphthene remains on the blade surface, indicating laminar boundary layer, only interrupted by narrow, wedge shaped areas of turbulent boundary layer. These wedges of turbulence originate from areas, where inadmissible large roughness force premature laminar-turbulent transition. The white area is followed by a region without coating of acenephthene. Here the thin, turbulent boundary layer with a very good heat transfer removes completely the acenaphthene. Downstream we see again white coated areas with acenaphthene. The reason is, that the turbulent boundary layer becomes thicker when developing downstream and the heat transfer becomes worse. During the ten minutes of hover flight the turbulent boundary layer in the sections ⑥ up to approximately ⑧ was not able, to sublimate the acenaphthene completely in the rear part of the blade. Structures in the white area of the rear part of the blade result from the varying thickness of the coating due to insufficient perfect spraying. Further Fig. 1 shows, that the laminar boundary layer is stable enough to overcome the disturbances in the surface of the blade at the end of the erosion cap without laminar-turbulent transition. The transition takes place more downstream.

It is obvious, that the extent of the laminar boundary layer becomes smaller for increasing values of relative rotor radius, because the local rotational speed and therefore the Reynolds number based on chord increases with radius.

Fig. 2 shows a detail from Fig. 1 for the sections ⑦ (r/R=0.82) to ⑨ (r/R=0.92). Interesting is a small detail between section ⑧ and ⑨ were we see an oblique joint in the erosion cap. The disturbance of the contour is so strong, that transition occurs on 2/3 of the width of this joint. Fig. 3 shows another detail of Fig. 1 for the sections ⑤ (r/R=0.69) to ⑦ (r/R=0.82). The Figures 2 and 3 show also, that the majority of the wedges of turbulence originate from disturbances, which are located in the front part of the erosion cap. During the operation of the helicopter it cannot be avoided that the cap will be damaged for example when grains of sand collide with the blade. These collisions produce small deformations of the cap which then become, depending on Reynolds number, intolerable rough surface areas. Thus, from the point of view of laminar flow, severe disturbances are found in an increasing number, investigating the blade from the roof to the tip. This is due to the fact, that the energy of particles in the outer part of the rotor is larger because of the larger rotational speed. Fig. 4 shows the complete lower blade surface from section ④ (r/R=0.62) to the tip. It can be seen clearly, that here also depending on the increasing Reynolds number with radius the extent of laminar boundary layer becomes shorter. Different to the results on the upper surface, the origin of most of the wedges of turbulence between the section ④ (r/R=0.62) and ⑧ (r/R=0.87) lies at the end of the erosion cap and its disturbances of the blade contour. For larger values of r/R the origins of the wedges of turbulence lie again on the cap itself. Due to the fact that the helicopter was in operation mostly in forward flight with high velocities and small or even negative angles of attack on the advancing blade, the upper surface of the nose region shows more severe and a larger number of damages than the lower surface. The contour disturbances in the transition between the cap and the rear part of the blade can be overcome by the boundary layer on the lower surface without direct laminar-turbulent transition. There are only some wedges of turbulence originating from the erosion cap because it is less eroded. The pressure distributions in hover flight have less favourate pressure gradients on the lower surface, so that the end of the cap often causes transition.

Details of the lower surface of the rotor blade are shown in Fig. 5 to 7. The clearness of flow visualization there suffers from a partly too thick coating of acenaphthene. In the outer part of the blade beginning at approximately r/R=0.87 the amount of surface area with laminar flow is strongly reduced.

5. Comparison of calculated points of transition with the experiment

5.1 Strategy and computer codes used

The calculation of the transition locations on a rotor blade is done using two-dimensional theory. In a first step the distribution of the local lift coefficients in hover flight along the blade radius were determined using a simulation code of DFVLR institute for flight mechanics [1].

Tab. 2 shows for sections ④ to ⑨ the values of local lift coefficients in hover flight as well as the corresponding Mach and Reynolds numbers. In each section the pressure distribution was calculated with the local free stream Mach number, the lift coefficient coming out of the simulation code and the Reynolds number based on the local chord. A two-dimensional, transonic computer code of Bauer/Garabedian/Korn/Jameson [2,3,4] in a modified version was used. In this code the turbulent boundary layer program of Nash McDonald [5] was replaced by a boundary layer code from Walz [6,7] for laminar and turbulent flow. In order to determine the laminar-turbulent transition location a modified criterion of Granville [8] was used. The method of Pretsch [9] allows the calculation of the friction induced pressure drag.

5.2 Results

Fig's 8 to 14 show for the sections ④ to ⑨ the calculated pressure distributions. The position of transition in experiment (arrow) and calculation is marked. A summary of the transition positions on upper and lower surface of the blade is given in Fig. 15. The calculated mean values of the transition location at different relative rotor radius positions are compared with results documented in the photographs. Except for section ⑩ on the upper surface, in the experiment longer laminar boundary layer is realized than in the calculation. On the lower surface however, the calculation shows at all sections a larger extent of laminar flow. Also, the difference between calculation and experiment at the lower surface becomes larger with increasing r/R. Nevertheless, the agreement is satisfactory taking into account all uncertainties. Tab. 2 summarizes the corresponding values.

Reasons for the discrepancies can be:

- Uncertainties in the transition criterion used in the calculation.
- Uncertainties in the calculation of the local pressure distribution due to uncertainties in the calculation of local, effective angle of attack.

- The influence on transition resulting from manufacturing tolerances of the contour and the rough transition from the erosion cap to the rear part of the blade are not taken into account.

- The evaluation of the transition position especially on the lower surface from the acenaphthene pictures is not fully sufficient.

- Three dimensional influences are neglected in the calculation.

6. Summary

The flow visualization using acenaphthene on a rotor blade in hover flight was found to be a fast and simple method, to determine the laminar-turbulent transition location.

Despite partially insufficient surface quality (especially in the front part of the blade), laminar boundary layers could be found on a large portion of the rotor blade surface. However, disturbances in the shape of the contour for example at the erosion cap must be avoided carefully. Also, periodical cleaning to remove insect debris is necessary for conservation of high aerodynamic performances of a blade. Calculations using a two-dimensional computer code showed satisfactory agreement with experimental transition location.

7. References

[1] v. Grünhagen, W. Das Hubschraubersimulationsmodell SIMH
DFVLR IB 111-85/21, Juni 1985

[2] Bauer, F.
Garabedian, P.
Korn, D. Supercritical Wing Sections
Springer Verlag Berlin/Heidelberg/New York, 1972.

[3] Bauer, F.
Garabedian, P.
Korn, D.
Jameson, A. Supercritical Wing Sections II.
Springer Verlag Berlin/Heidelberg/New York, 1975.

[4] Bauer, F.
Garabedian, P.
Korn, D. Supercritical Wing Sections III.
Springer Verlag Berlin/Heidelberg/New York, 1977.

[5] Nash, J.F.
McDonald,
A.G.J. The calculation of Momentum Thickness in a Turbulent Boundary Layer at Mach Number up to Unity.
A.R.C. CP No. 963, (1967).

[6] Rohardt, C.-H. Erweiterung eines Nachrechnungsverfahrens für zweidimensionale transsonische Strömungen durch ein leistungsfähiges Grenzschichtverfahren.
DFVLR IB, 1983.

[7] Walz, A. Strömungs- und Temperaturgrenzschichten.
Verlag G. Braun, Karlsruhe, 1966.

[8] Granville, P.S. The calculation of the Viscous Drag of Bodies of Revolution.
David Taylor Model Basin, Rep. No. 848, 1953.

[9] Pretsch, J. Zur theoretischen Berechnung des Profilwiderstandes.
Jahrbuch 1938 d. dt. Luftfahrtforschung, S. I 60-I 81.

Airfoil	:	NACA 23012 MOD.
Blade condition	:	approx. 450 hours of operation, exhaust gas residues and insect debris removed from surface
Blade chord	:	0.28 m
Number of rotor revolutions	:	425 RPM
Rotor radius	:	R = 4.92 m
Air temperature	:	13 °C
Duration of the experiment	:	2 minutes alignment and warm up, $c_A \approx 0$ 10 minutes of hover flight 2 minutes cool down, $c_A \approx 0$
Flow visualization	:	Acenaphthene

Table 1: Conditions of Experiment

Section No.	r/R	c_a	Ma	$Re/10^6$	Experiment x/l Transition Upper Surface	Experiment x/l Transition Lower Surface	Corresponding Pressure Distribution in Figure No.	Calculation x/l Transition Upper Surface	Calculation x/l Transition Lower Surface
4	0.62	0.56	0.40	2.60	-	0.73	8	0.180	0.770
5	0.69	0.57	0.44	2.89	0.24	0.72	9	0.170	0.760
6	0.75	0.56	0.48	3.15	0.24	0.65	10	0.170	0.740
7	0.82	0.56	0.53	3.44	0.22	0.61	11	0.170	0.715
8	0.87	0.55	0.56	3.65	0.22	0.56	12	0.160	0.680
9	0.92	0.53	0.59	3.86	0.18	0.41	13	0.160	0.640
10	0.97	0.52	0.63	4.07	0.11	0.39	14	0.175	0.620

Table 2: Evaluation of Transition Position from Photographs on a BO 105 Rotor Blade in Hover Flight and Comparison with Calculation

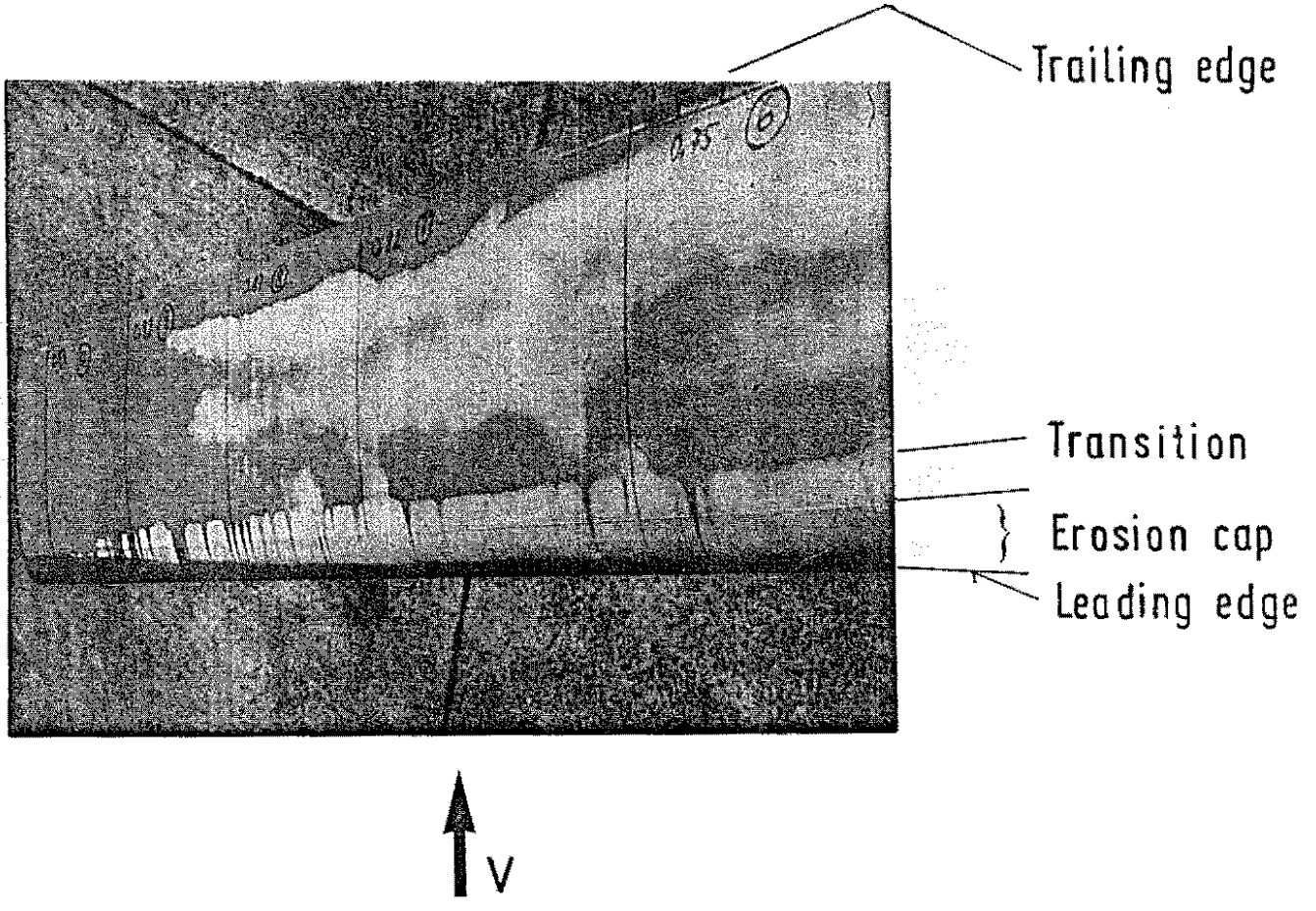

Fig. 1 BO 105, Detail of Rotor Blade,
Upper Surface $0.69 \leqq r/R \leqq 1.0$

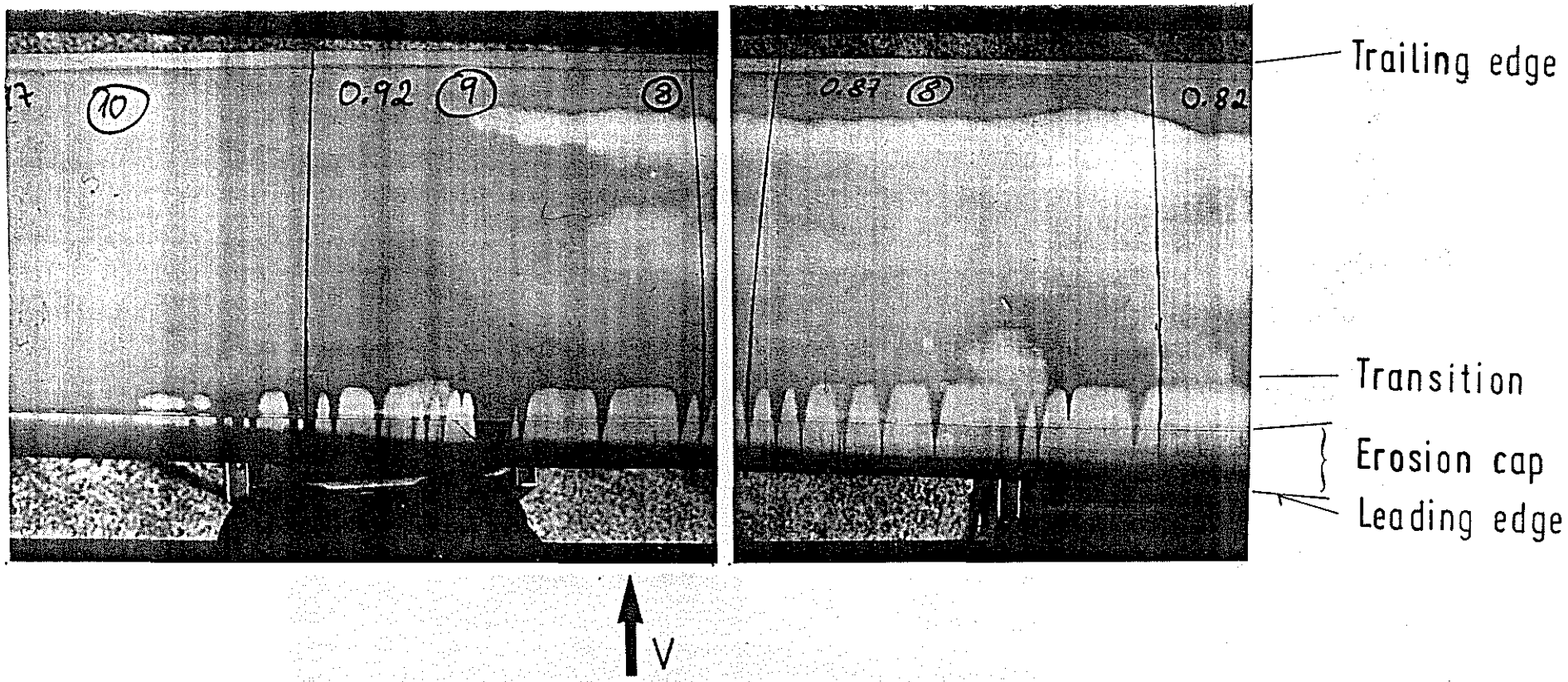

Fig. 2 BO 105, Detail of Rotor Blade, Upper Surface $0.82 \leqq r/R \leqq 0.97$

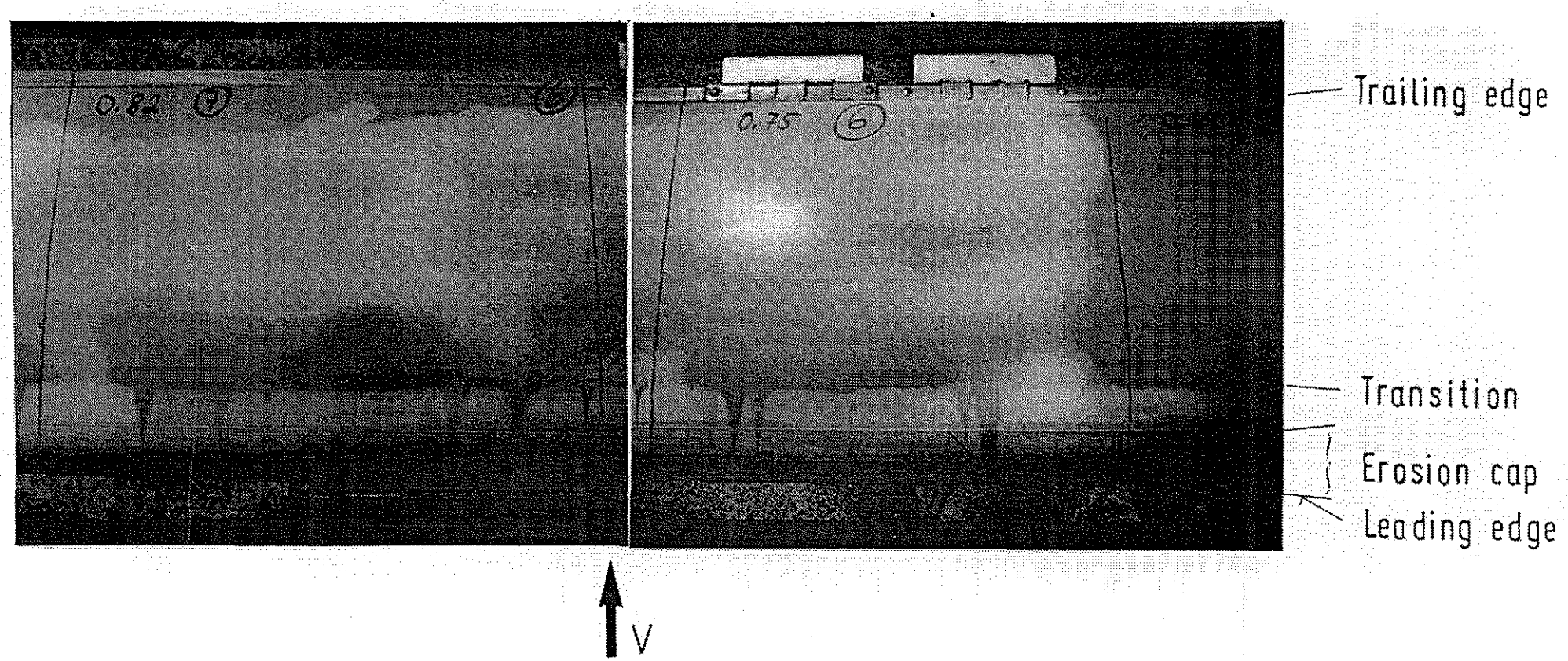

Fig. 3 BO 105, Detail of Rotor Blade, Upper Surface $0.69 \leqq r/R \leqq 0.82$

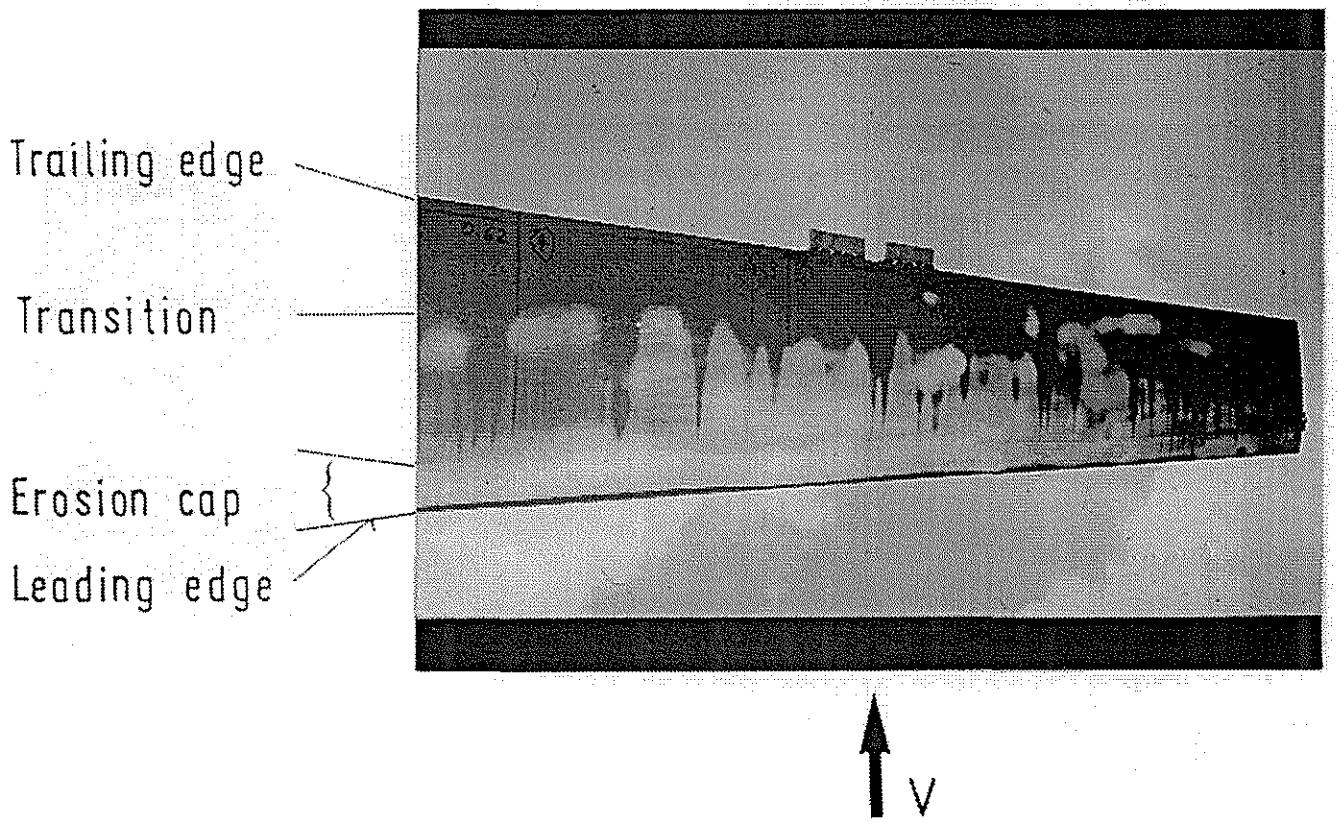

Fig. 4 BO 105, Detail of Rotor Blade, Upper Surface $0.62 \leqq r/R \leqq 1.0$

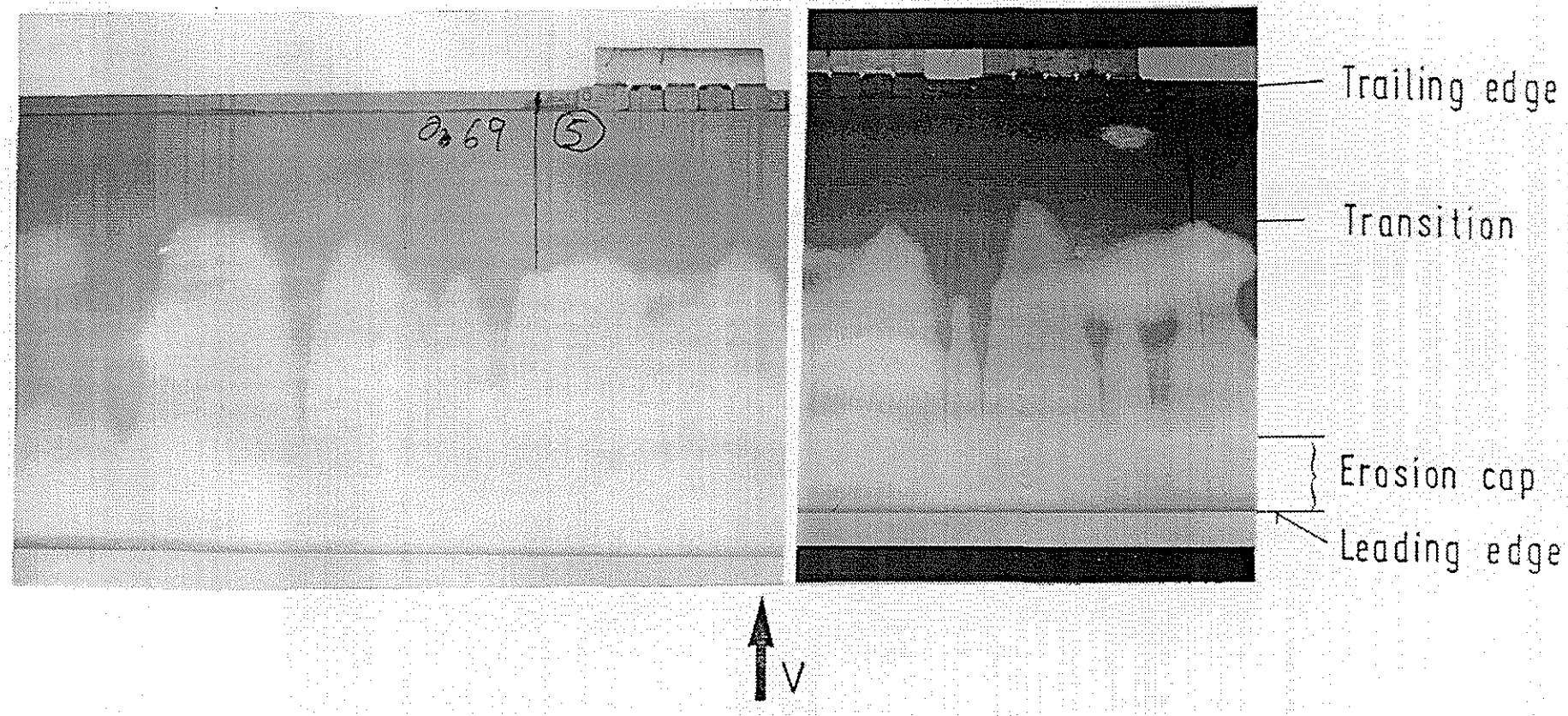

Fig. 5 BO 105, Detail of Rotor Blade, Lower Surface $0.62 \leqq r/R \leqq 0.75$

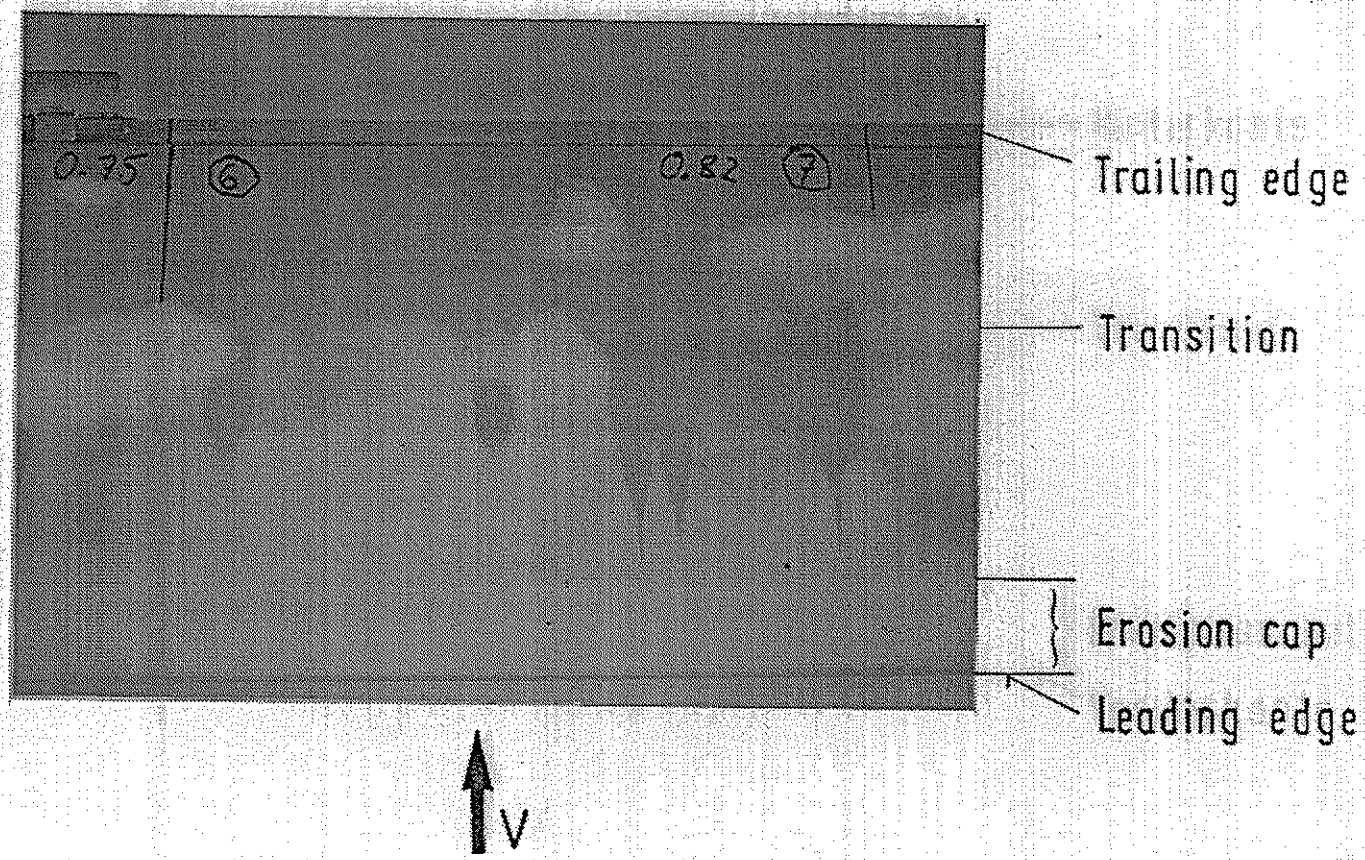

Fig. 6 BO 105, Detail of Rotor Blade,
Lower Surface $0.75 \leqq r/R \leqq 0.82$

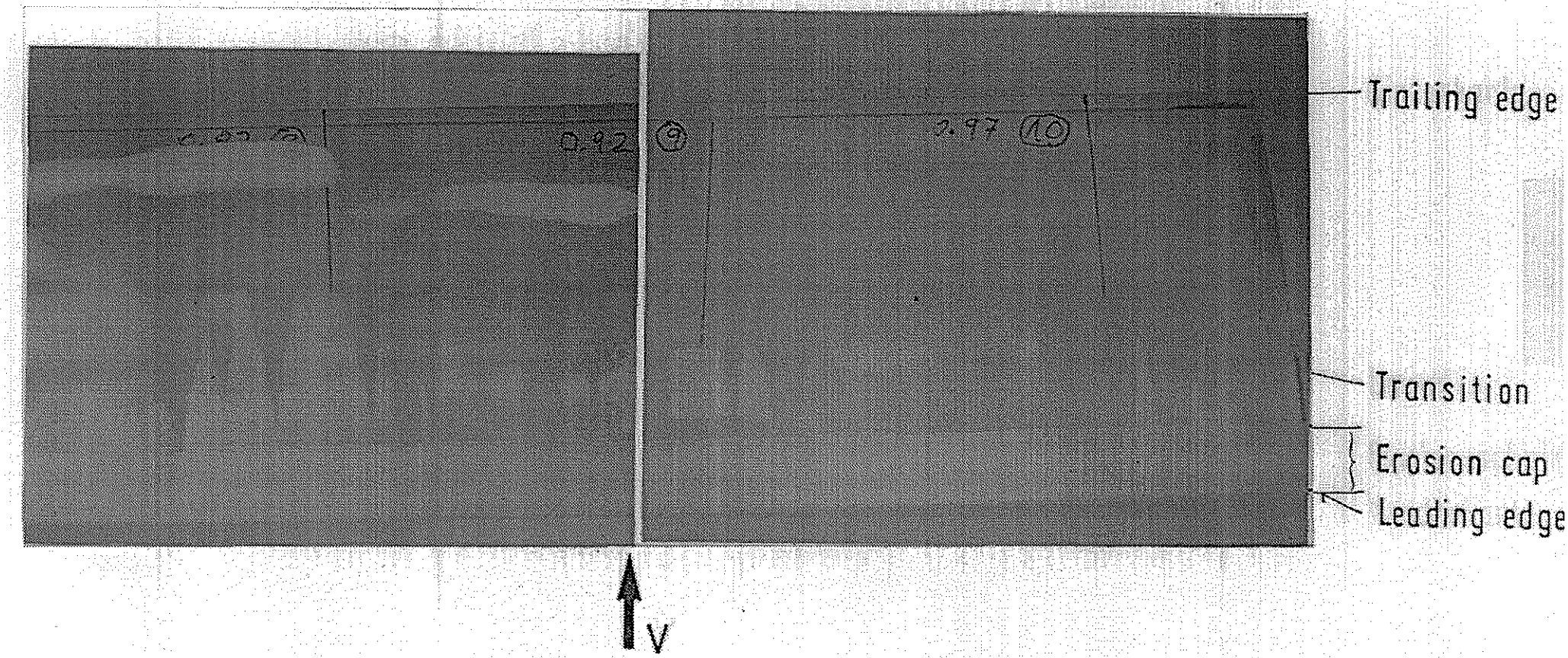

Fig. 7 BO 105, Detail of Rotor Blade, Lower Surface $0.87 \leqq r/R \leqq 0.97$

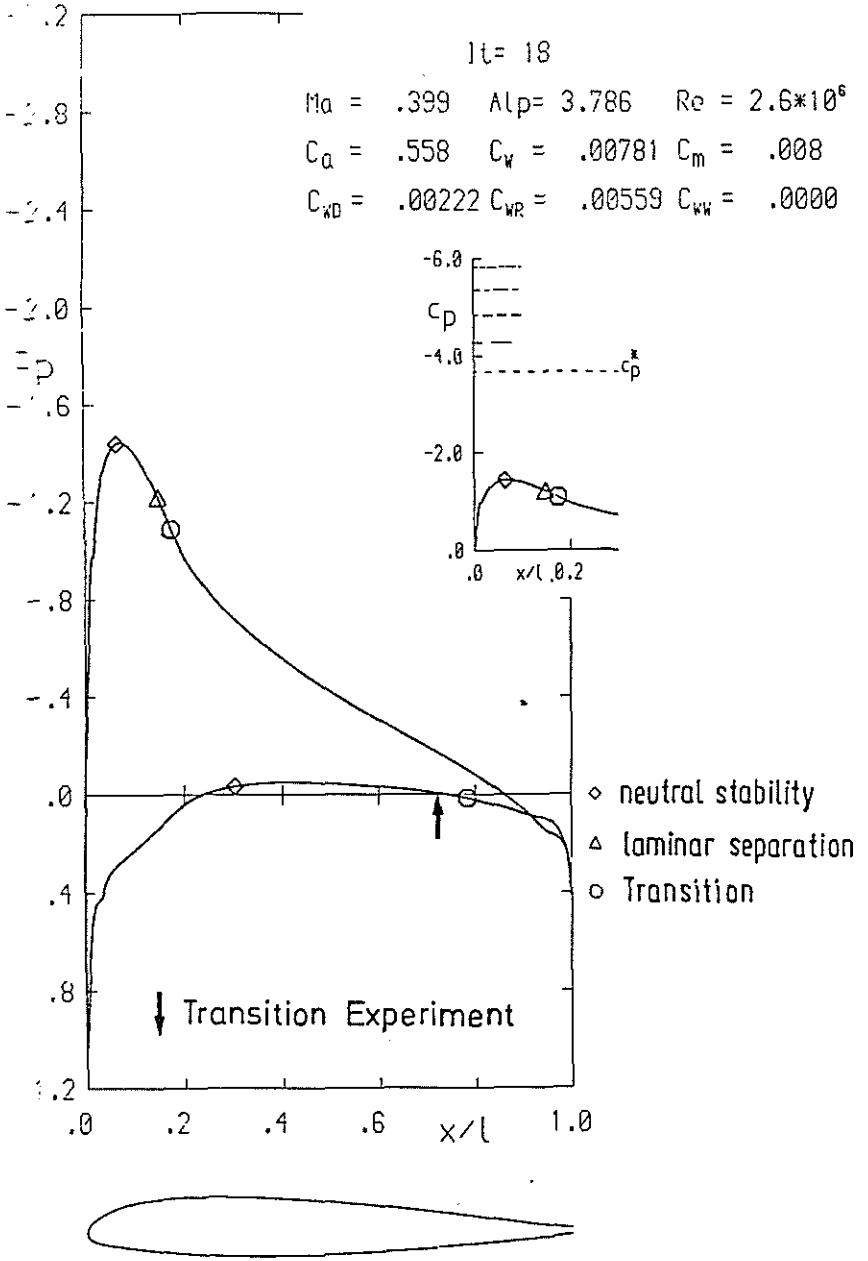

Fig. 8 Pressure Distribution Airfoil NACA 23012.MOD
Section ④ , r/R = 0.62

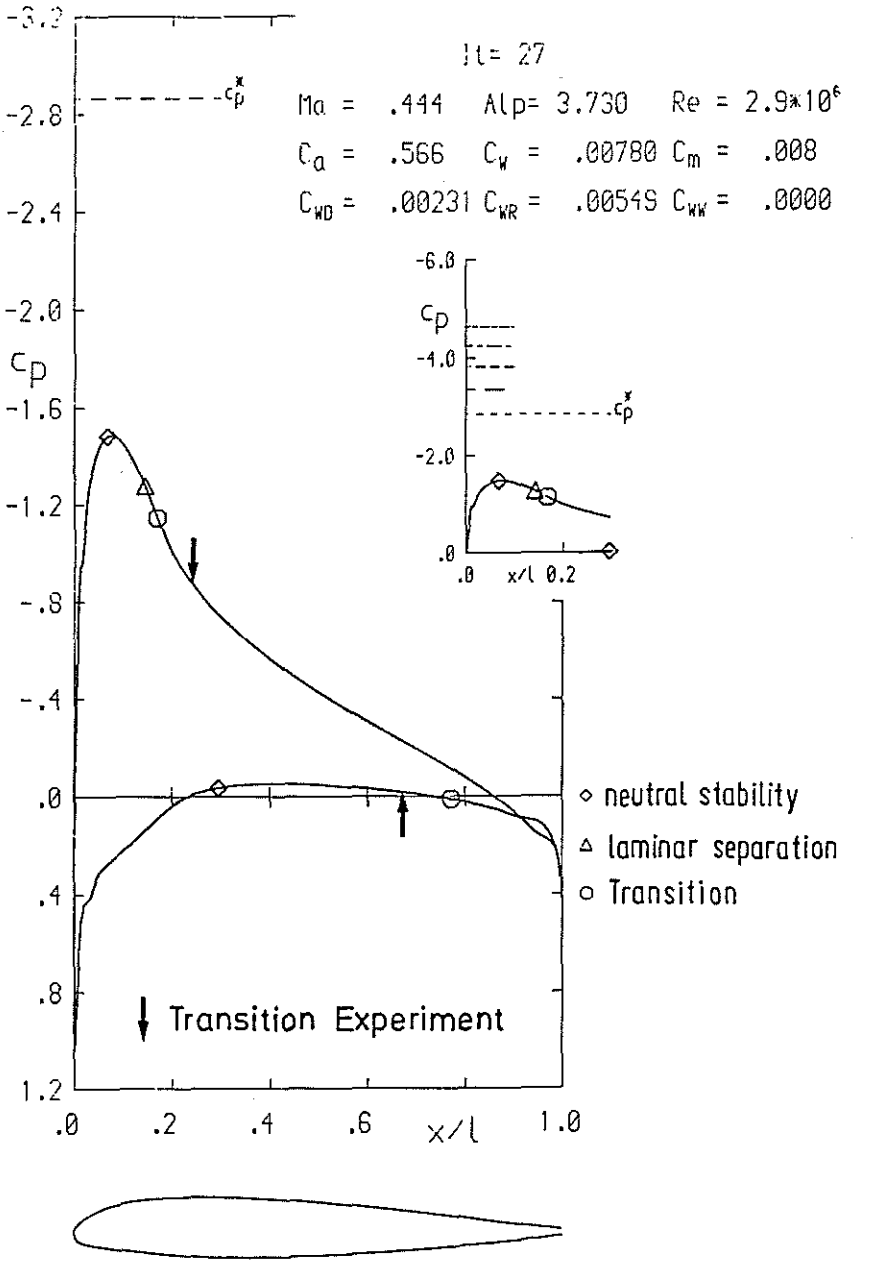

Fig. 9 Pressure Distribution Airfoil NACA 23012.MOD
Section ⑤ , r/R = 0.69

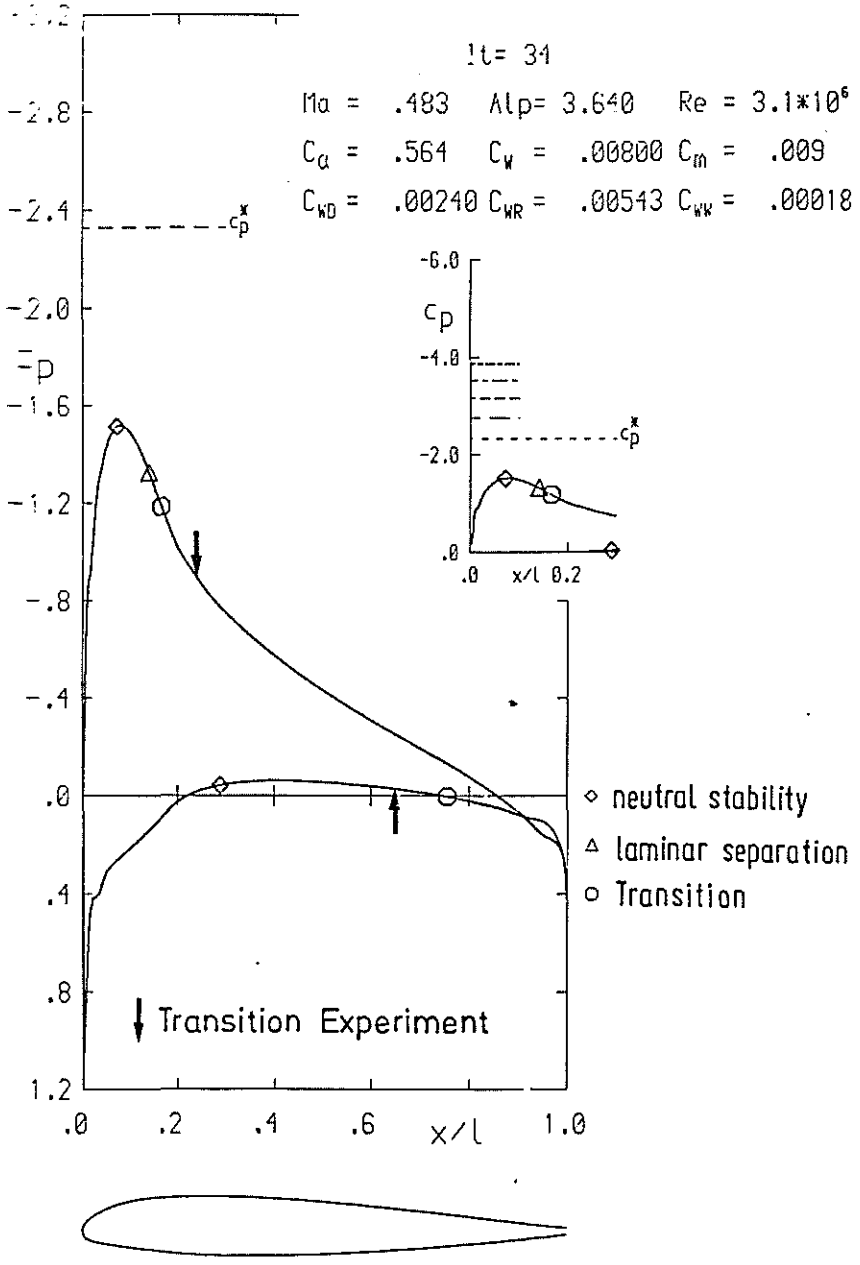

Fig. 10 Pressure Distribution Airfoil NACA 23012.MOD
Section ⑥, r/R = 0.75

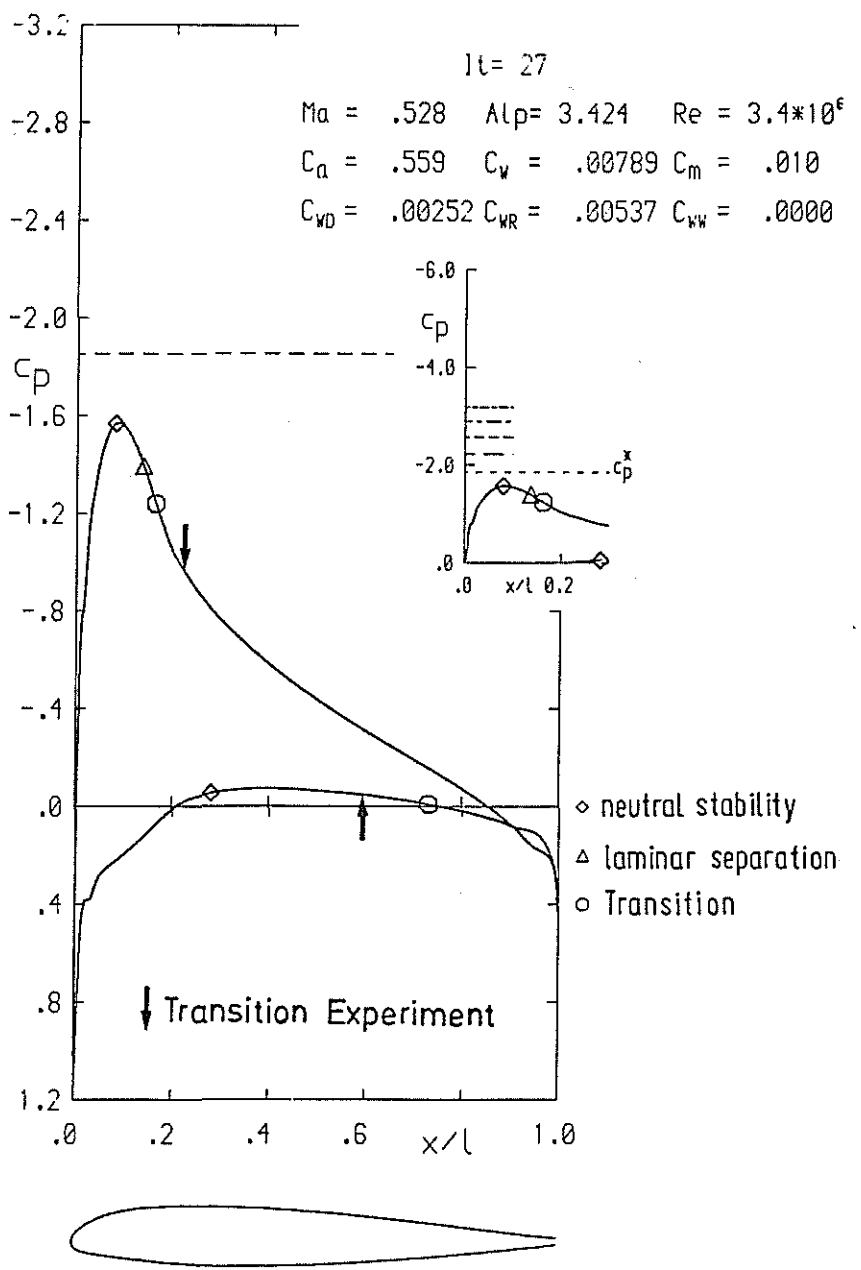

Fig. 11 Pressure Distribution Airfoil NACA 23012.MOD
Section ⑦, r/R = 0.82

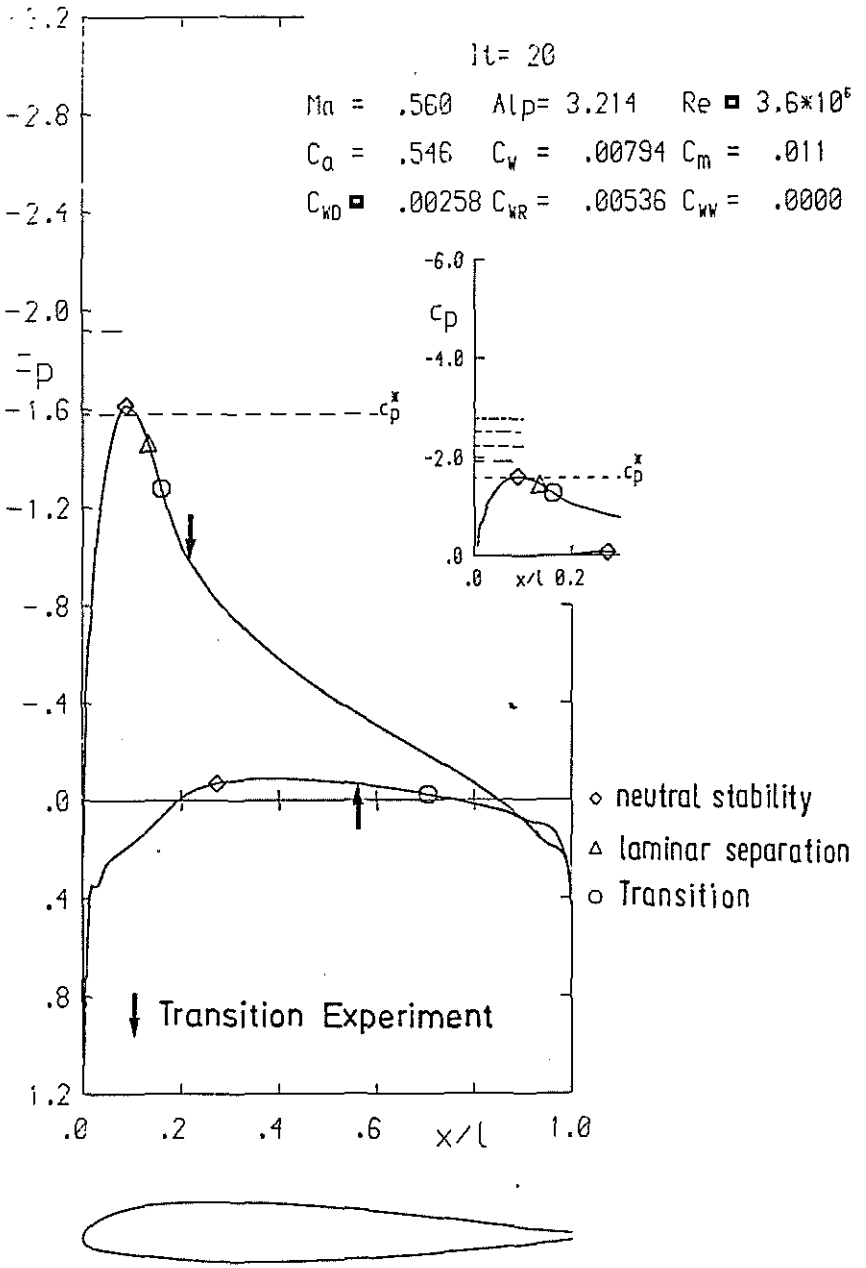

Fig. 12 Pressure Distribution Airfoil NACA 23012.MOD
Section ⑧ , r/R = 0.87

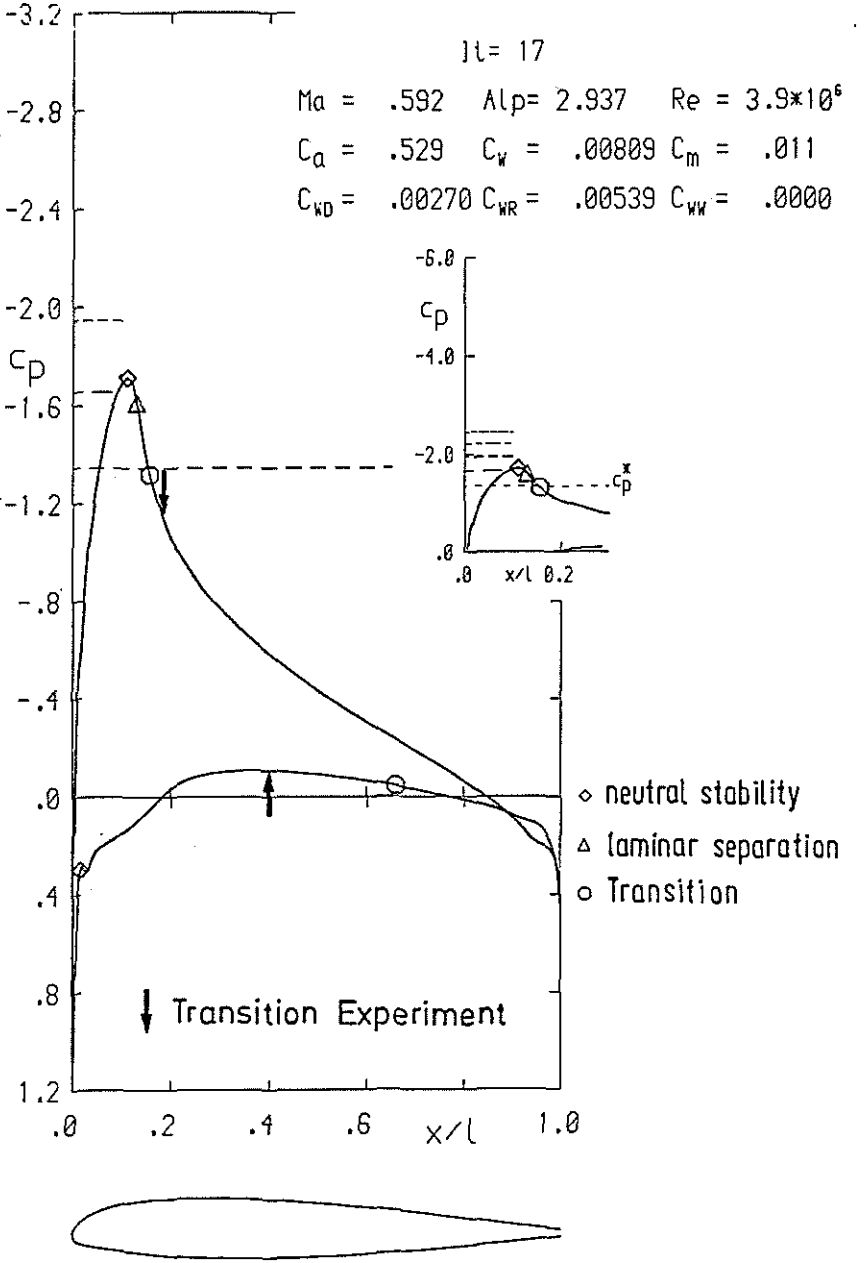

Fig. 13 Pressure Distribution Airfoil NACA 23012.MOD
Section ⑨ , r/R = 0.92

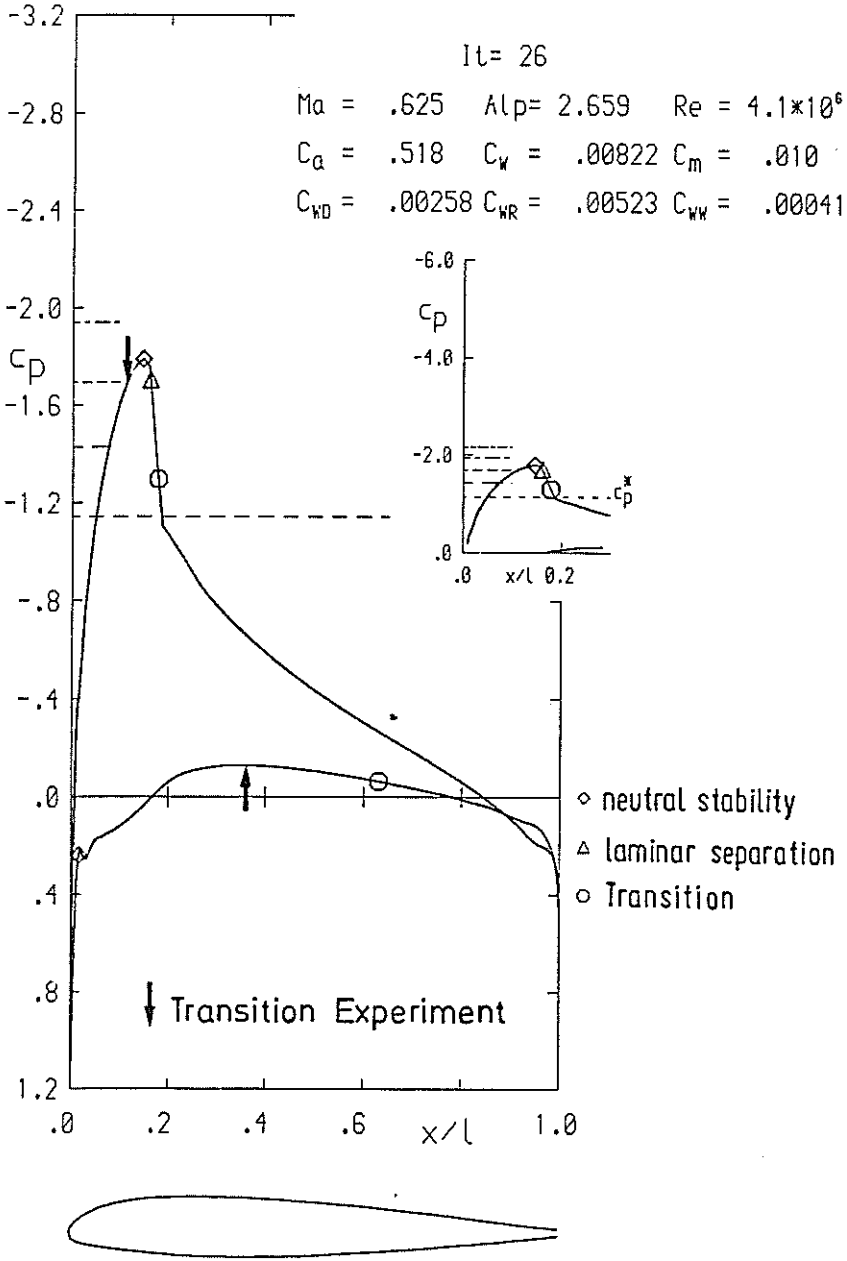

Fig. 14 Pressure Distribution Airfoil NACA 23012.MOD
Section (10), r/R = 0.97

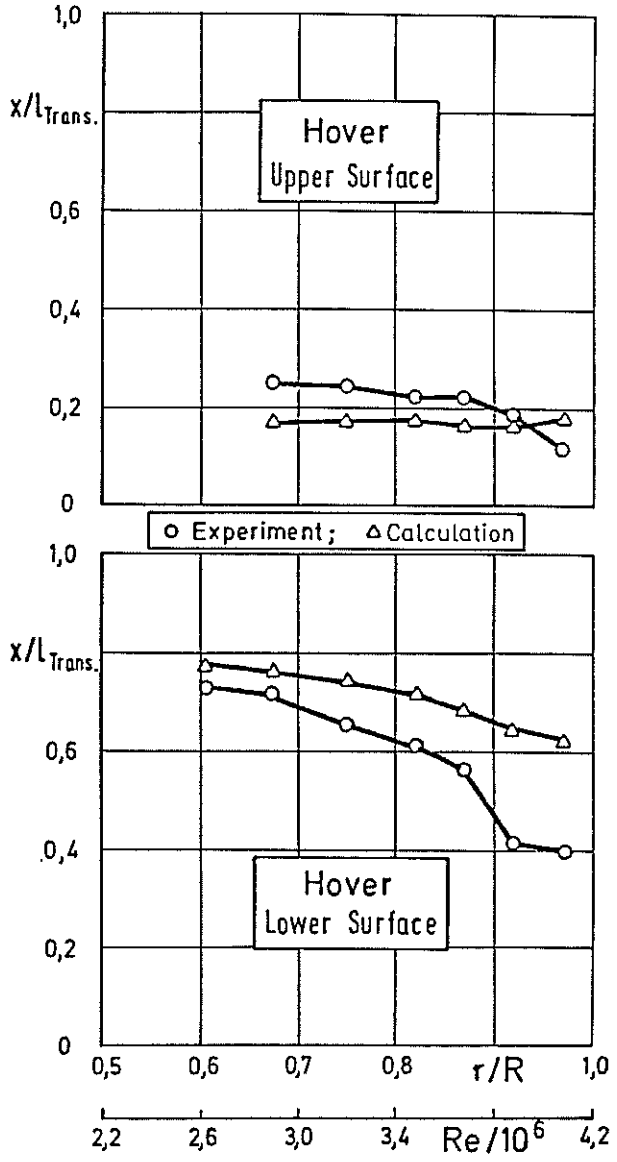

Fig. 15 Position of Laminar-Turbulent Transition